Hindawi
Advances in Civil Engineering
Volume 2021, Article ID 8651467, 15 pages
https://doi.org/10.1155/2021/8651467

Research Article

Experimental Study on the Influence of Freezing Pressure on the Uniaxial Mechanical Properties of Ice

Baosheng Wang,[1,2] **Weihao Yang**,[2] **Peixin Sun**,[2] **Xin Huang**,[2] **Yaodan Zhang**,[3] **and Fengjun Chen**[1]

[1]*Shanghai Construction Group Co., Ltd., Shanghai 200080, China*
[2]*State Key Laboratory for Geomechanics and Deep Underground Engineering, China University of Mining and Technology, Xuzhou 221116, China*
[3]*State Key Laboratory of Coastal and Offshore Engineering, Dalian University of Technology, Dalian 116024, China*

Correspondence should be addressed to Baosheng Wang; wangbs@scg.cn

Received 15 July 2021; Accepted 9 August 2021; Published 20 August 2021

Academic Editor: Xiaohu Zhang

In this study, a test technique that enables continuous control of the sample stress state from freezing to testing is proposed to investigate the influence of freezing pressure on the mechanical properties of ice under uniaxial compression. In this method, the water is frozen into the standard cylindrical ice specimen under high hydraulic pressure in a triaxial pressure chamber, and then, the temperature field and stress field of the ice specimens are adjusted to the initial state of the test; finally, an in situ mechanical test is conducted in the triaxial chamber. The uniaxial compression test of ice specimens with temperature of −20°C and freezing pressure of 0.5–30 MPa is performed in the strain rate range of 5×10^{-5}–1.5×10^{-6} s^{-1}. The results show that, as the freezing pressure increases, the ductile-to-brittle transition zone of the ice specimen during failure moves to the low strain rate range, and the failure mode of the specimen changes from shear failure to splitting failure. Further, the brittleness index of the ice specimen first increases, then decreases, and then again increases with the increase in freezing pressure. The brittleness index reaches the maximum (minimum) when the freezing pressure is 30 MPa (20 MPa). The peak stress of the ice specimen also increases first, then decreases, and then increases with the increase in freezing pressure. The maximum value is also at the freezing pressure of 30 MPa, but the minimum value is obtained at the freezing pressure of 0.5 MPa. The failure strain of the ice specimen first decreases and then increases with the increase in freezing pressure, and the maximum (minimum) value is achieved at the freezing pressure of 0.5 MPa (10 MPa). When the ice specimen exhibits brittle failure, the relationships between the residual stress and the freezing pressure and between the peak stress and freezing pressure are the same, but when the ice specimen exhibits ductile failure, there is no obvious relationship between the residual stress and the freezing pressure.

1. Introduction

Artificial ground freezing method is the most important construction method to stabilize the ground and prevent groundwater ingress during excavation. It allows the penetration of deep, unstable, and water-bearing strata containing sands, silts, and clays. Presently, the depth of artificially frozen topsoil and water-rich strata has reached 750 m [1] and 950 m [2], respectively. The measured data show that the static [3] and dynamic [4] mechanical responses of deep frozen wall are quite different from the theoretical expectations due to the lack of understanding of the formation mechanism of deep frozen soil and rock mass. At present, the deepest proven natural permafrost layer is more than 1 km deep [5]. Due to the influence of high pressure in the deep environment, there are still many difficulties in drilling and coring in deep permafrost layer [6]. To solve these problems, the mechanical properties of deep frozen soil [7–9] and frozen rock [10, 11] have been experimentally investigated, but the research on the coupling problems of ice-soil and ice-rock, which are based on the mechanical properties of deep-environment ice, is not

mature. Compared with the shallow layer conditions, the deep formation pressure increases significantly [12–14], and the freezing pressure of the deep groundwater can exceed 10 MPa due to the high pressure and the limit on the formation of frost heaving. Therefore, it is of great significance to examine the influence of freezing pressure on the mechanical properties of ice.

Vostok subglacial lake in Antarctica is the deepest lake on the Earth. The thickness of the overlying ice sheet is nearly 4 km [15]. Due to its long history and complete isolation from the outside world, the water of this lake water has significant research value. To obtain lake water specimens, a Russian research team has started the drilling project of huge thick ice sheet since the beginning of this century. However, due to the lack of understanding of the mechanical response of the bottom ice layer, sudden lake water gushing frequently occurs while drilling the bottom of the ice sheet, which brings great difficulties to the sampling process [16]. Isotopic studies have shown that the bottom ice layer is frozen by the high-pressure lake water [17]. Therefore, revealing the mechanical properties of ice frozen at high pressure can boost the applications of drilling technology of thick ice sheet. In addition, there is a high-pressure freezing phenomenon in hydrous exoplanets. For example, the liquid water of Europa is stored under a 150 km thick ice shell, and the high-pressure water is constantly frozen into ice at the bottom of the ice shell [18]. As the observation of ice shell rheology is one of the principal means to explore the extraterrestrial liquid water resources, whether freezing pressure affects the rheological characteristics of ice is worth to be studied.

The uniaxial compression test is a simple method that has been widely used to study the mechanical properties of ice. Using this test, the enhancement effect of negative temperature on the ice strength [19, 20] and stiffness [21, 22], the influence of the loading rate on the failure characteristics [23, 24] and its mechanism [25, 26], and the ductile-brittle transition of ice failure under different conditions [27, 28] have been investigated. However, the ice used in the above studies was frozen without any pressure. There are few reports on mechanical properties of ice frozen under pressure. Furthermore, in the existing technique to form ice by freezing pure water, the water is slowly and unidirectionally frozen to form a large ice body by controlling the heat flow gradient in a large volume, low temperature tank [29–31], and then, the core is taken and processed into a cylindrical ice specimen. This method can realize pressure freezing by improving the equipment, but the ice specimen needs pressure relief, drilling, and grinding. In this process, the stress state of the ice specimen is uncontrollable, and nonideal condition such as instantaneous removal of freezing pressure will inevitably be produced, leading to microcracks and other defects in the ice specimen [32], which cannot fully reflect the effect of pressure freezing.

To address the above issues, in this study, an effective method is proposed to freeze the cylindrical water specimen in a triaxial pressure chamber to form a standard cylindrical ice specimen. Then, the temperature field and stress field of the ice specimen are adjusted to the initial condition of the test, and the in situ mechanical test is performed to realize the continuous control of the stress state of the specimen during the entire process of freezing and testing. The proposed method is used to prepare ice specimens with freezing pressure from 0.5 MPa to 30 MPa, and uniaxial compression tests are conducted at a constant strain rate and temperature of −20°C. Furthermore, the effects of freezing pressure on the constitutive laws and strength characteristics of the ice specimens are investigated.

2. Experimental Method

2.1. Testing Equipment. The test method prepared in this study is based on the in situ test method of high-pressure frozen geotechnical materials. The entire process of pressure freezing and mechanical test is conducted in a triaxial pressure chamber. The experimental equipment is TAS-LF400 low-temperature triaxial system, which is jointly developed by China University of Mining and Technology and Xi'an KTL Instruments Co., Ltd., as shown in Figure 1. The ultimate axial force of the loading frame is 400 kN, the maximum confining pressure of the pressure/volume controller is 64 MPa, and the control accuracy is 0.05%. The temperature field of the specimen is controlled by the three circulation channels at the top, side, and bottom of the triaxial pressure chamber and the constant, low-temperature circulation grooves A, B, and C connected with them, respectively. The minimum temperature is 60°C, and the temperature control accuracy is 0.1°C. Two lead holes are arranged on the side wall of the pressure chamber to install the sealed lead connector of the sensor.

2.2. Preparation Technique of Ice Specimens

2.2.1. Freezing Process. The ice specimen was prepared by freezing the cylindrical water specimen in the triaxial pressure chamber [33]. The size of the water specimen was $\Phi 61.8 \times 114.7\ \text{mm}^2$. Using the control technology, the freezing expanded by 9% [34] would be forced to develop along the height direction, and the ice specimen with the target size of $\Phi 61.8 \times 125\ \text{mm}^2$ was obtained. The controlled freezing process was divided into two stages: specimen pressurization and stable pressure freezing. During the pressurization, the height of the water specimen was kept constant by the load frame to avoid concave folds due to axial compression, and the confining pressure was increased to the target pressure value by the pressure volume controller. In the period of stable pressure freezing, the quantity of the confining medium in the triaxial chamber was locked by the pressure volume controller to force the freezing expansion to develop along the height direction of the specimen, and the specimen pressure is then controlled by the load frame, which is set to apply a constant axial pressure. The water specimen froze in a gradient temperature field of cold in the lower and hot in the upper generated by circulation thermostats A and C. The radial deformation of the specimen is restricted by the stable volume of the confining medium, and the freezing expansion develops along the height direction as the expansion pressure releases.

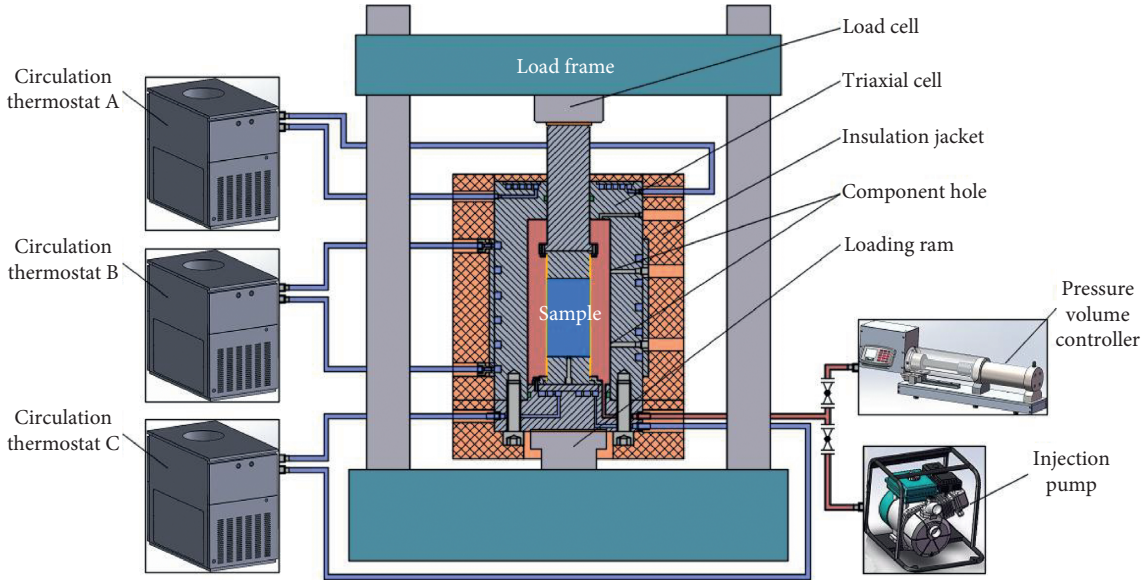

Figure 1: Sketch of the TAS-LF400 low-temperature triaxial testing system.

The ice specimen after freezing is shown in Figure 2. The diameter is measured three times from the bottom of the ice specimen along the upward axis, and each measurement is taken along the specimen's circumferential interval of 120° (Figure 3(a)). The measurement results (Figure 3(b)) indicate that the maximum and minimum diameters of the ice specimen are 62.01 and 61.68 mm, respectively, and the maximum absolute error and the maximum relative error of the radial size are 0.33 mm and 0.5%, respectively, which meet the test specifications for geometric accuracy [35].

2.2.2. Temperature Field Adjustment. Ice is a temperature-sensitive material, and its temperature distribution has a significant effect on the mechanical properties. To obtain the real temperature field of the ice specimen, the joint temperature measurement of distributed optical fiber and thermal resistance was employed, and the corresponding layout is shown in Figure 4.

The fiber was sealed in a carbon fiber tube with a diameter of 3 mm and placed along the axis of the specimen. The tube prevented the disturbance of pressure circumstance on the test results. The thermal conductivity of the carbon fiber material is relatively low, meaning that the original temperature distribution of the ice specimen would not be interfered [36]. The distributed optical fiber test equipment was the ODiSI Measurement System, LUNA Company, which could measure the temperature distribution along the whole fiber length, and the temperature measurement accuracy was 0.1°C. Three thermal resistors were arranged along the axial direction outside the insulation film of the specimen, and the temperature measurement accuracy was 0.05°C. The radial temperature distribution of the specimen could be simultaneously analyzed with the measurement results of the optical fiber and the thermal resistors.

Since the ice specimen was formed by one-way freezing from bottom to top, the temperature distribution at the completion of freezing was cold in the lower and hot in the upper. Before the test, the temperature field needed to be adjusted to uniform distribution according to the design temperature. The design temperature of the test was −20°C, and the temperature field was adjusted by using the three constant low-temperature circulation tanks A, B, and C (Figure 1). In the adjustment process, seven temperature measuring points with equal spacing were set on the distributed optical fiber (Figure 4) to monitor the variation in the temperature field of the ice specimen. The measurement results (Figure 5) indicate that the temperature field of the ice specimen reaches a stable state after approximately 8 h. The measured temperature values of the distributed optical fiber and thermistor in the steady state are shown in Figure 6. The final temperature of the ice specimen is slightly higher in the center and slightly lower at both the ends and sides. The difference between the internal maximum temperature and the minimum temperature is 0.51°C, and the average temperature is −20.08°C, which meets the test specifications.

2.2.3. Stress Field Adjustment. Before the test, the stress state of ice specimen should be changed from the pressure freezing state to the initial state. It is necessary to limit the stress state and variation rate in the conversion process to avoid cracks [37, 38]. According to the triaxial test conclusion of Kalifa et al. [39], when the loading rate is lower than 1 MPa/s, ice begins to crack when the deviatoric stress reaches 0.25–0.5 times the ultimate deviatoric stress. The unloading experiments of Couture and Schulson [40] suggested that the unloading rate should not be greater than 0.17 MPa·s^{-1} to ensure that cracks do not appear in the ice specimen. In this study, a more conservative constraint is adopted, i.e., the deviatoric stress should not be greater than 0.2 times the ultimate deviatoric stress during the process of stress state transformation, and the adjustment rates of axial pressure and confining pressure should not be greater than 0.05 MPa·s^{-1}.

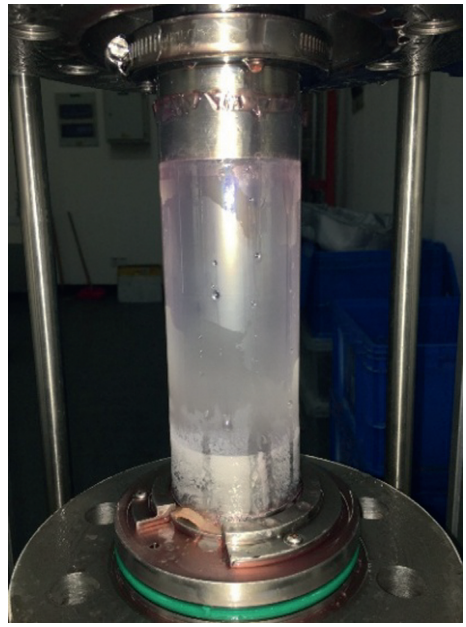

Figure 2: An ice sample frozen by the pressurized freezing technique.

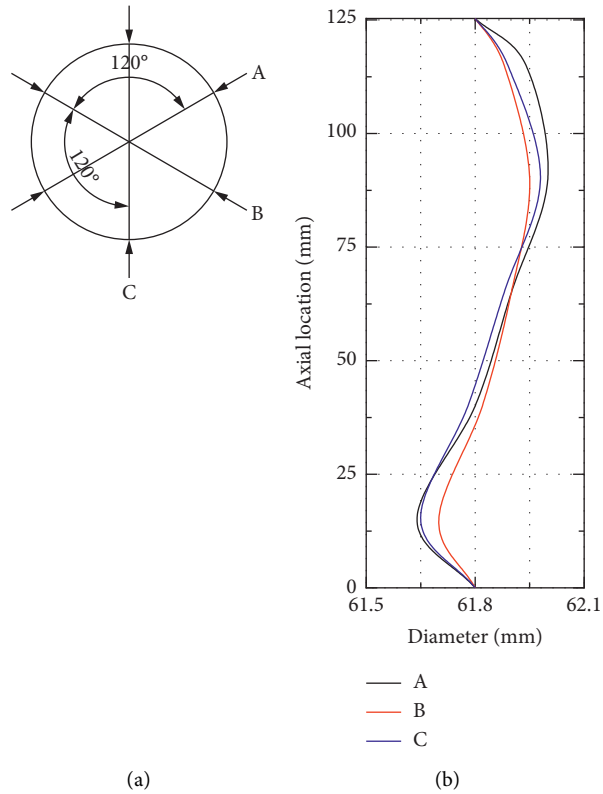

Figure 3: Ice sample diameter: (a) measurement intervals and (b) measurement results.

2.3. Experimental Procedures. Using the above specimen preparation technique, in situ uniaxial compression tests of pressurized freezing ice were conducted at −20°C under the constant strain rate. The strain rates considered were 5×10^{-5}, 1.5×10^{-5}, 5×10^{-6}, and 1.5×10^{-6} s^{-1}. Since the radial accuracy of the ice specimen relies on the interaction between the specimen and the confining medium during freezing, the pressure applied in the freezing process cannot be less than 0.5 MPa. Therefore, the freezing pressure of ice specimens was set to 0.5, 10, 20, and 30 MPa. The test was

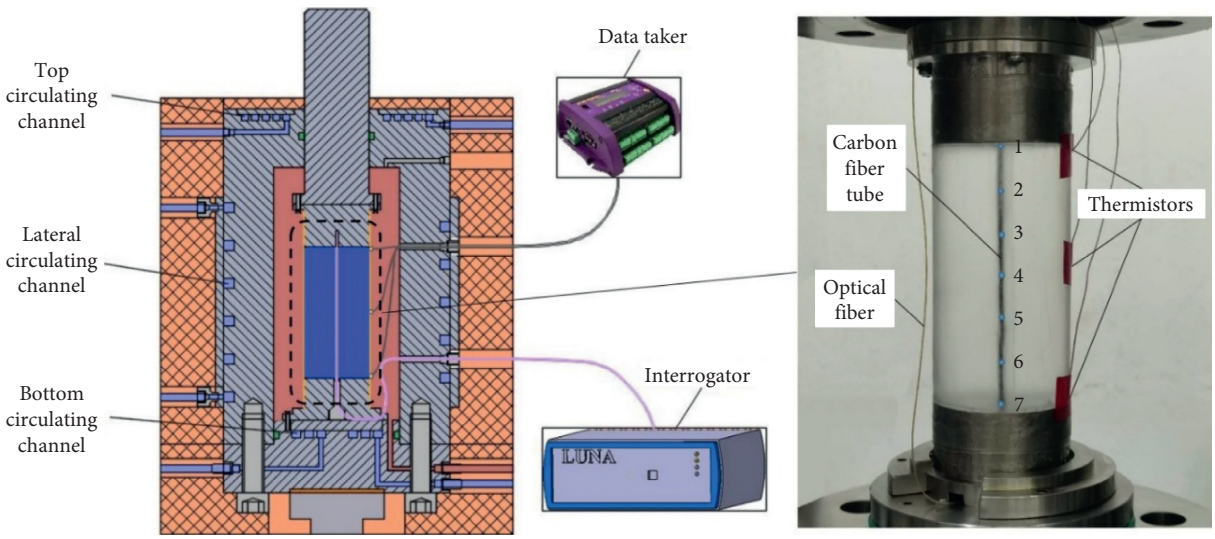

Figure 4: Arrangement of temperature sensors.

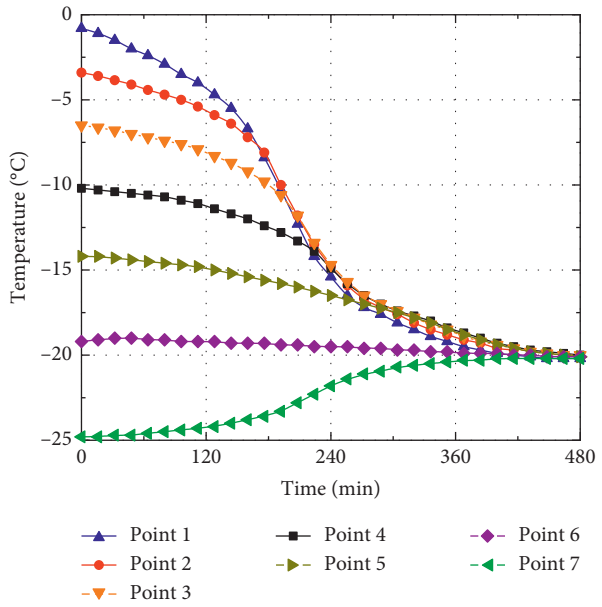

Figure 5: Variation in the temperature of seven measurement points on the optical fiber with time.

conducted using all the combinations of the above parameters. Each group contained two specimens, and a total of 32 specimens were tested.

The specific test process is as follows: firstly, the ice specimen was frozen under the pressure environment by using the controlled freezing process. Then, keeping the freezing stress field unchanged, the temperature field of the ice specimen was adjusted to a uniform value of −20°C. After the temperature field of the ice specimen became stable, the freezing pressure of the ice specimen was removed at the rate of 0.05 MPa·s^{-1} under the condition that the three-dimensional pressures are equal. The uniaxial compression test with the constant strain rate was immediately conducted after the unloading process.

3. Results and Discussion

The stress-strain curves for all the 32 groups of tests are classified and summarized according to the freezing pressure in Figure 7. The test conditions and characteristic results corresponding to each curve are shown in Table 1. The curves with the same test conditions are represented in the same color, and the two repetitions are distinguished by different markers (circles and triangles). According to Table 1, the repeated errors of peak stress, failure strain, and residual stress of the test under the same conditions are 4–14%, 0–14%, and 0–8%, respectively, which are lower than most of the earlier reported values for ice uniaxial compression tests [41–44] and are close to the repeated errors of

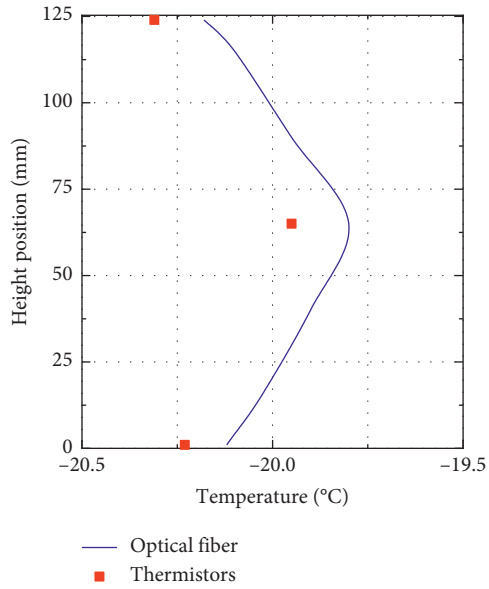

Figure 6: Measurement results of the optical fiber and thermistor under the stable temperature field of the ice specimen.

precisive tests carried out by Ramseier [45]. The above results prove that the proposed test technique is reliable with high control precision and strong repeatability.

3.1. Stress-Strain Behavior

3.1.1. Failure Characteristics. Due to the rheological properties of ice, the failure characteristics after loading deformation are closely related to the strain rate. When the strain rate is slow, there is sufficient time for dislocation sliding between the ice crystals, so the stress-strain relationship of ice is elastoplastic, leading to ductile failure. When the strain rate is fast, the dislocation sliding between the ice crystals cannot occur, resulting in the dominant internal cracking and crushing. The stress-strain curve drops suddenly after reaching the peak, and brittle failure occurs. In Figure 7(a), when the strain rate is 5×10^{-5} s^{-1}, the failure characteristics of ice specimens with freezing pressure of 0.5 MPa exhibit one brittle and one ductile, while the ice specimens with high pressure freezing all show brittle failure, which indicates that the influence of freezing pressure on the failure characteristics of ice is similar to that of low temperature, leading to the ductile-to-brittle transition zone move to a slow strain rate range.

The specific failure pattern is shown in Figure 8. After the test was completed, hydraulic oil was discharged while maintaining the low temperature in the pressure chamber, and then, the ice specimen was taken out, which took nearly 1 h. In the above process, the side of the ice specimen was tightly wrapped by a heat shrink tube, and the internal cracks were healed to a certain extent under the effect of recrystallization, resulting in self-repair of the ice specimen that might have been disintegrated due to compression failure. Therefore, all the damaged ice specimens were still continuous after the heat shrink tube was removed. The typical failure images of each specimen were processed using Photoshop software to make the internal cracks clearer. These images are shown in Figures 8(a)–8(d), which reveal the variation in the failure mode of ice specimens under freezing pressure of 0.5–30 MPa and different strain rates. When the freezing pressure is low, there are fewer cracks inside the ice specimen, forming a vertical or inclined main crack (see Figure 8(b) for 0.5 MPa and Figure 8(d) for 0.5 MPa). As the freezing pressure increases, the number of cracks in the specimen gradually increases (see Figure 8(a) for 10 MPa), forming a certain fracture zone in the specimen (see Figure 8(c) for 20 MPa). In addition, with the increase in the freezing pressure, the crack concentration at the top and bottom of the specimen becomes increasingly obvious (see Figure 8(c) for 30 MPa). At a low strain rate, the specimens with high freezing pressure show lateral bulging failure (see Figure 8(d) for 30 MPa), and at high strain rate, the specimens with high freezing pressure still tend to exhibit shear failure (see Figure 8(a) for 30 MPa). In general, as the freezing pressure increases, the failure mode of the ice specimen changes from shear failure to splitting failure, and as the strain rate increases, this phenomenon becomes more and more obvious.

3.1.2. Brittleness Index. The test specimens with strain rates of 1.5×10^{-5}–1.5×10^{-6} s^{-1} all showed ductile failure, and all the constitutive curves revealed strain-softening characteristics, but the rates of prepeak rise and postpeak decline of the curves were significantly affected by the freezing pressure. The stress variation rate of the constitutive curve is closely related to the brittleness of the material, which can be quantitatively evaluated by the brittleness index [46, 47]. There are four ways to extract the brittleness index according to the total stress-strain curve (Table 2), and the greater the index, the more significant the brittleness of the material. The index B_1 was proposed by Bishop [48], who suggested that the brittleness of the material can be characterized by

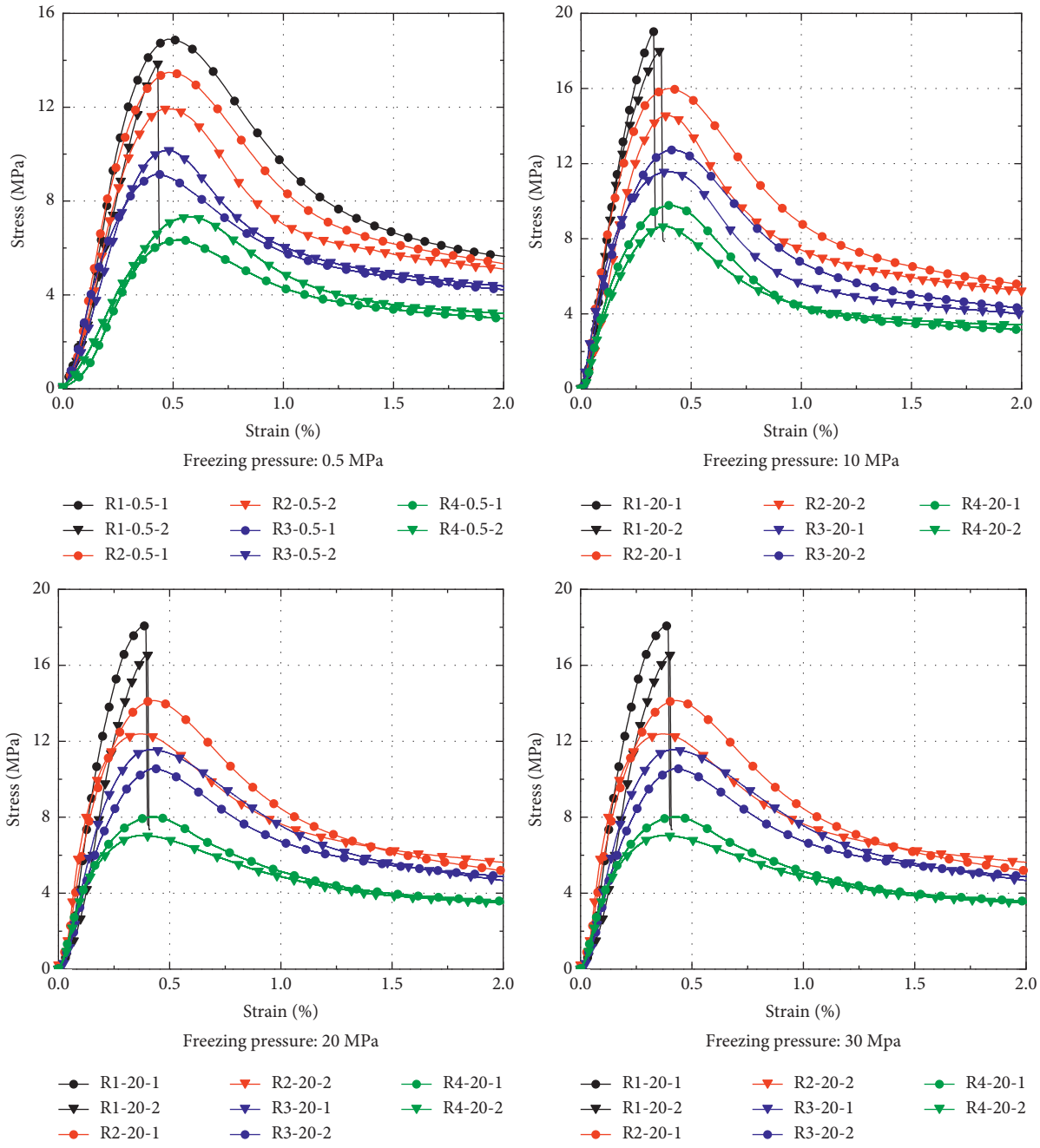

Figure 7: Stress-strain curves of all experiments.

the stress drop amplitude after the failure of the specimen, namely, the ratio of the postpeak drop of the stress to the peak stress. Subsequently, Zhou et al. [49] considered the absolute deceleration based on the relative magnitude of the postpeak stress drop and took its logarithm value as the coefficient to propose another brittleness index B_2. Xia et al. [50] considered the influence of the prepeak stress-strain state on the brittleness characteristics; they used the ratio of the elastic energy released during the specimen failure to the total deformation energy stored before the peak to characterize the brittleness index. Based on the deformation energy calculation method of Tarasov and Potvin [51], the index B_3 was derived. Tarasov and Potvin [51] believed that the brittleness degree should be reflected by the relative relationship between the deformation energy of the specimen before and after the peak of the constitutive curve, and the index can be expressed by the relationship between the modulus parameters before and after the peak, namely, B_4.

The brittleness indices are calculated according to Table 2, where the modulus parameters are shown in Table 3. The calculated brittleness index is shown in Figure 9. Under all the strain rates, the variation in the four brittleness indexes with the freezing pressure is similar: the indexes increase first, then decrease, and then again increase. The mean

Table 1: Experimental conditions and results.

Group	Strain rate (s^{-1})	Freezing pressure (MPa)	Peak stress (MPa)	Failure strain	Residual stress (MPa)	Failure types
R1-0.5-1	5×10^{-5}	0.5	14.90	0.48	5.63	Ductile
R1-0.5-2		0.5	13.85	0.43	6.13	Brittle
R1-10-1		10	19.00	0.33	8.48	Brittle
R1-10-2		10	18.12	0.36	7.83	Brittle
R1-20-1		20	18.10	0.39	7.52	Brittle
R1-20-2		20	16.54	0.40	7.59	Brittle
R1-30-1		30	19.55	0.41	9.65	Brittle
R1-30-2		30	20.33	0.40	10.07	Brittle
R2-0.5-1	1.5×10^{-5}	0.5	13.50	0.48	5.33	Ductile
R2-0.5-2		0.5	11.92	0.46	5.16	Ductile
R2-10-1		10	16.00	0.40	5.54	Ductile
R2-10-2		10	14.55	0.38	5.23	Ductile
R2-20-1		20	14.14	0.42	5.17	Ductile
R2-20-2		20	12.39	0.37	5.62	Ductile
R2-30-1		30	17.21	0.45	5.51	Ductile
R2-30-2		30	16.10	0.43	5.80	Ductile
R3-0.5-1	5×10^{-6}	0.5	9.14	0.43	4.22	Ductile
R3-0.5-2		0.5	10.17	0.48	4.25	Ductile
R3-10-1		10	12.73	0.40	4.14	Ductile
R3-10-2		10	11.58	0.40	4.31	Ductile
R3-20-1		20	10.55	0.41	4.88	Ductile
R3-20-2		20	11.57	0.43	4.66	Ductile
R3-30-1		30	14.03	0.45	4.88	Ductile
R3-30-2		30	13.02	0.43	4.84	Ductile
R4-0.5-1	1.5×10^{-6}	0.5	6.35	0.53	2.99	Ductile
R4-0.5-2		0.5	7.33	0.51	3.04	Ductile
R4-10-1		10	9.79	0.40	3.15	Ductile
R4-10-2		10	8.65	0.37	3.43	Ductile
R4-20-1		20	8.02	0.42	3.57	Ductile
R4-20-2		20	7.04	0.36	3.78	Ductile
R4-30-1		30	10.62	0.45	3.43	Ductile
R4-30-2		30	9.92	0.42	3.42	Ductile

value of the four brittleness indexes increases in the following order of the freezing pressure:

$$\overline{B}(20\,\text{MPa}) < \overline{B}(0.5\,\text{MPa})\overline{B}(10\,\text{MPa}) < \overline{B}(30\,\text{MPa}), \quad (1)$$

where $\overline{B}$ is the arithmetic average value of $B_1 - B_4$. The number in the brackets represent the freezing pressure.

The brittleness index calculated according to the constitutive relation can reflect the deformation law of ice under static load, which provides a basis for engineers to predict the deformation trend of frozen wall. In addition, the brittleness index is an important parameter to evaluate the dynamic response. The material with the higher brittleness index is easier to be cracked under dynamic action.

When the freezing method is used to construct the shaft in deep water-rich strata, the drilling and blasting method is needed to excavate the inner space of the shaft. Figure 9 shows that according to the hydrostatic head difference, the brittleness of ice at a depth of 1000 meters is significantly greater than that at the shallow part, which should be cautious in the design of the blasting process; particularly, the layout of the surrounding holes should be optimized to avoid the potential safety hazards caused by the cracking and leakage of the frozen wall. The variation in the ice brittleness with the depth can also play a role in effective drilling of thick ice cover. Engineers can improve the bit form according to the variation in the brittleness index, and the drilling pressure, rotation speed, and other parameters in the drilling process can be optimized to improve the ice breaking efficiency.

3.2. Mechanical Properties

3.2.1. Peak Stress. According to the test, the variation in the peak stress as a function of the freezing pressure is shown in Figure 10. The scattered points are the measured values of each group of tests. The fold lines represent the change in the average value of the repeated test results. The colors of the points and lines correspond to the strain rate. Under the same freezing pressure, the peak stress of ice specimen increases with the increase in the strain rate, which is consistent with the test results of nonpressure freezing ice within the same strain rate range [28, 52]. Under the four strain rates, the variation laws of the peak stress of ice specimens are similar, and the peak stress does not monotonically change with the increase in the freezing

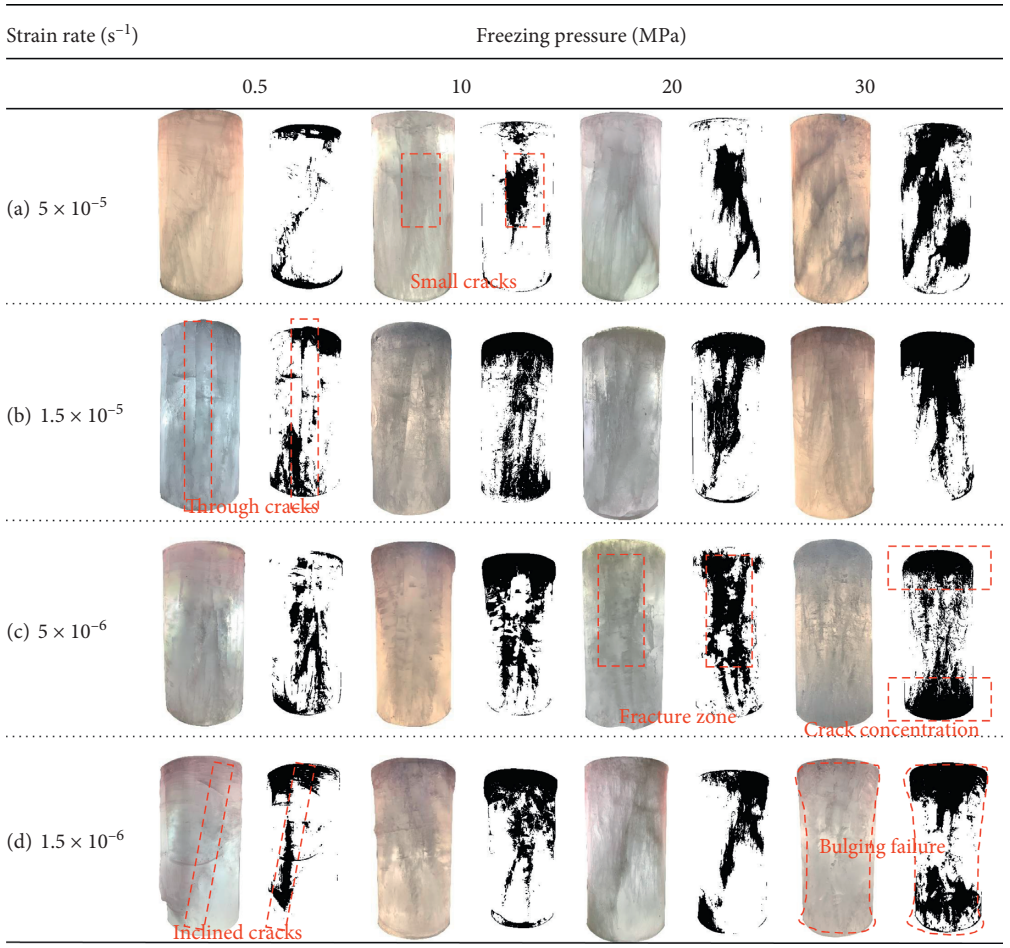

Figure 8: Failure pattern of representative specimens. (a)5×10^{-5}. (b)1.5×10^{-5}. (c)5×10^{-6}. (d)1.5×10^{-6}.

Table 2: Summary of calculation methods for the brittleness index.

Formula	Meaning of parameters
$B_1 = \sigma_P - \sigma_r/\sigma_P$	B is the brittleness index; the lower number represents different representation; σ_P and σ_r are peak stress and residual stress, respectively
$B_2 = \sigma_P - \sigma_r/\sigma_P \lg\lvert k_{ac}\rvert/10$	k_{ac} is the absolute deceleration after peak , that is, $k_{ac} = \sigma_P - \sigma_r/\varepsilon_r - \varepsilon_P$
$B_3 = \sigma_P - \sigma_r/\varepsilon_r - \varepsilon_P + (\sigma_P - \sigma_r)(\varepsilon_r - \varepsilon_P)/\sigma_P\varepsilon_P$	ε_P and ε_r are failure strain and residual strain, respectively
$B_4 = E_{tb} - E_{ta}/E_{tb}$	$E_{tb,E_{ta}}$ are maximum tangent modulus before and after peak

pressure, but it increases first, then decreases, and then again increases. When the freezing pressure increases from 0.5 MPa to 10 MPa, the average peak stress increases by 2.50–4.19 MPa, and the relative increase is 20–38%. When the freezing pressure rises to 20 MPa, the peak stress does not continue to rise, and its average value decreases by 1.10–2.01 MPa with a relative decrease of 6–20%. When the freezing pressure increases to 30 MPa, the peak stress increases again, and the average value is 2.47–3.39 MPa higher than that at 20 MPa, and the relative increase is 15–36%.

The freezing pressure interval selected in this experiment is large, and the freezing pressures of 10 MPa and 20 MPa are not necessarily the inflection points of the continuous variation curve of uniaxial compressive strength of ice specimens. It is necessary to conduct more detailed research by narrowing the interval to obtain comprehensive and accurate variation law. However, the dashed line rule of Figure 10 is still valuable for engineering applications and scientific research. Taking the artificial freezing project as an example, the groundwater pressure is calculated according to the head difference. The test results show that the strength of artificial freezing ice increases significantly with the increase in depth in the depth range of 0–1000 m. These results can provide a basis for decreasing the thickness of pure ice bearing wall of artificial freezing engineering in deep karst [53] and deep water [54], which can reduce energy consumption and shorten the construction period. In addition, ice, as an important part of rock and soil frozen wall, largely determines the mechanical properties of frozen wall. Therefore, the variation law of compressive strength of

Table 3: Summary of the maximum tangent modulus before and after the peak of stress-strain curves.

Group	Strain rate (s^{-1})	Freezing pressure (MPa)	Prepeak maximum tangent modulus E_{tb} (GPa)	Maximum tangent modulus after peak E_{ta} (GPa)
R2-0.5-1	1.5×10^{-5}	0.5	6.06	1.36
R2-0.5-2		0.5	6.00	1.28
R2-10-1		10	8.16	1.92
R2-10-2		10	7.95	2.11
R2-20-1		20	8.02	1.28
R2-20-2		20	7.75	1.01
R2-30-1		30	8.78	1.70
R2-30-2		30	8.42	1.52
R3-0.5-1	5×10^{-6}	0.5	5.06	1.01
R3-0.5-2		0.5	4.55	0.79
R3-10-1		10	7.53	1.67
R3-10-2		10	7.80	1.50
R3-20-1		20	6.28	0.89
R3-20-2		20	5.26	0.89
R3-30-1		30	8.80	1.49
R3-30-2		30	7.39	1.60
R4-0.5-1	1.5×10^{-6}	0.5	3.60	0.89
R4-0.5-2		0.5	3.04	0.57
R4-10-1		10	5.07	1.37
R4-10-2		10	4.88	1.13
R4-20-1		20	4.03	0.77
R4-20-2		20	4.33	0.58
R4-30-1		30	5.16	1.25
R4-30-2		30	5.05	1.30

frozen ice can play a crucial role in the study of ice-rock or ice-soil coupling problems and improving the utilization rate of bearing capacity of deep frozen wall.

3.2.2. Residual Stress. The variation in the residual stress of ice specimens with freezing pressure at different strain rates is shown in Figure 11. At the high strain rate, the variation in the residual stress with freezing pressure is consistent with that of the peak stress because the ice specimen exhibits brittle failure in this condition (Figure 7). The value of residual stress is the fall point of the stress-strain curve, and the mechanism through which the freezing pressure affects the stress value is still the same as that for the peak stress. When the strain rate decreases, the failure mode of the ice specimen transforms into ductile failure, and the residual stress is changed to the stable stress value dropping from the peak of the stress-strain curve. In this case, the residual stress of the ice specimen does not change significantly with the increase in freezing pressure.

In artificial freezing construction in thick alluvium, the frozen wall is often in a low-speed rheological state, and the deformation is large, which can reach more than 5% in severe cases [3]. In this case, the bearing capacity of the frozen wall is reflected in its residual strength. Combined with the variation law of peak stress (Figure 10) and residual stress (Figure 11) of ice with the freezing pressure, it can be seen that, under the condition of small deformation, the resistance of freezing wall increases significantly with the increase in depth, which is conducive to reducing the thickness of freezing wall. However, after entering the stage of large deformation, the bearing capacity advantage of deep frozen wall disappears, resulting in accelerated deformation under high ground pressure, which is unfavorable to the construction safety. Therefore, in the deep topsoil freezing project, it may be useful to adjust the height of the construction section and shorten the exposure time of the frozen wall to limit the deformation of the frozen wall, which may facilitate the bearing capacity advantage.

3.2.3. Failure Strain. The variation in the failure strain with freezing pressure is shown in Figure 12. Different from the change law of stress strength, there is no obvious relationship between the failure strain and the strain rate, which is consistent with the experimental results for nonpressure freezing ice in the same strain rate range [28, 51]. Under the four strain rates, the failure strain decreases first and then increases with the increase in the freezing pressure. When the freezing pressure is 0.5 MPa, the failure strain is the maximum, and its value

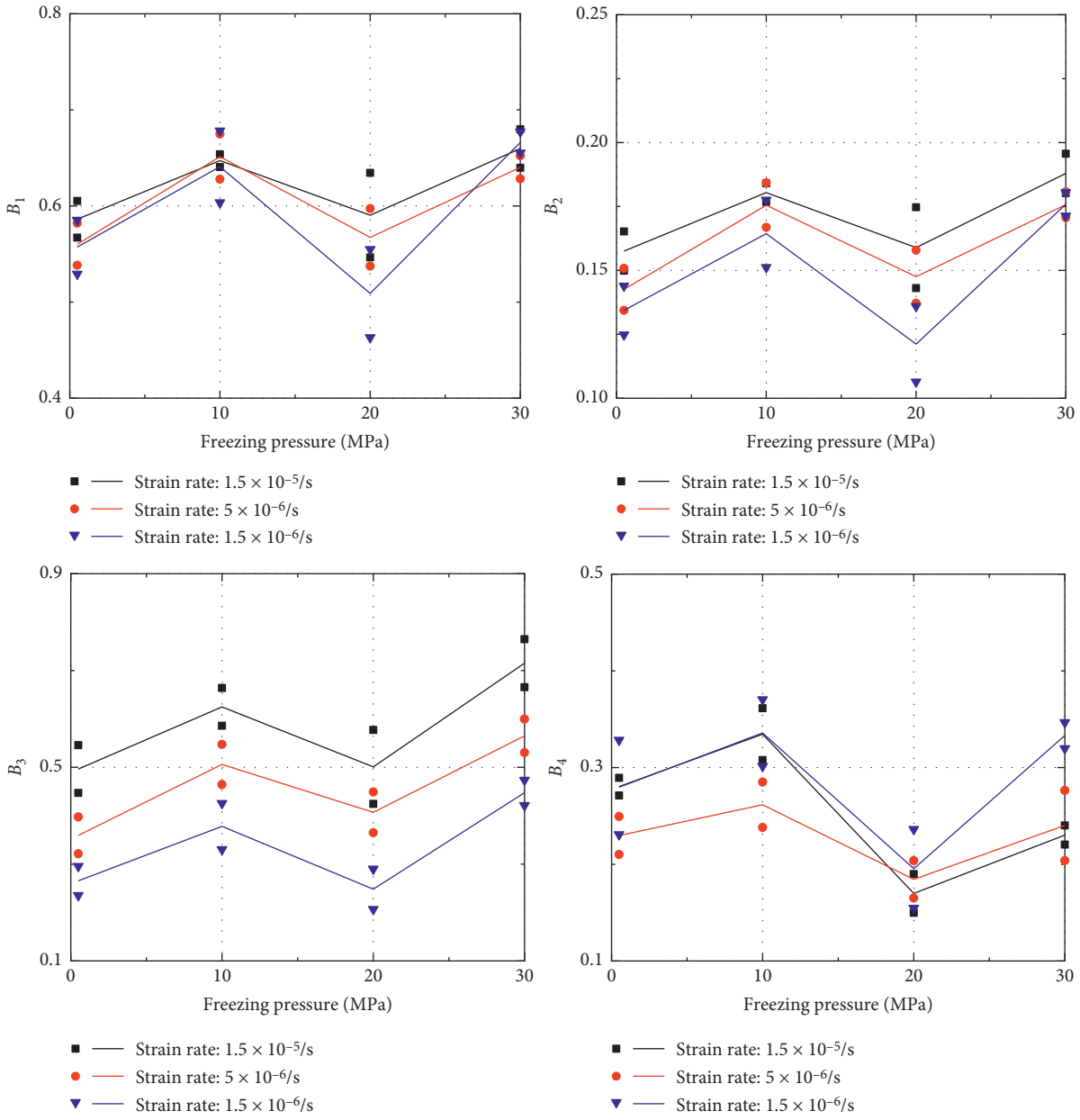

Figure 9: Variation in the brittleness indexes with freezing pressure under different strain rates.

is between 0.43% and 0.53%, which is consistent with the failure strain of pressureless frozen ice [28, 51, 55]. When the freezing pressure rises to 10 MPa, the failure strain decreases to a minimum of 0.33–0.4%. Then, the failure strain increases to 0.36–0.43% and 0.40–0.45% when the freezing pressure rises to 20 MPa and 30 MPa, respectively, but it is still lower than the test results of ice specimen frozen under the pressure of 0.5 MPa.

As mentioned in Section 3.2.1, the freezing pressure of 10 MPa is not necessarily the lowest point of the continuous variation curve of failure strain, but the fold line law of failure strain is still worthy of attention of engineers. Since the freezing pressure significantly reduces the failure strain of ice, it is likely that the deformation of the frozen wall formed under high pressure enters the plastic stage too early. Especially, when the groundwater pressure reaches 10 MPa,

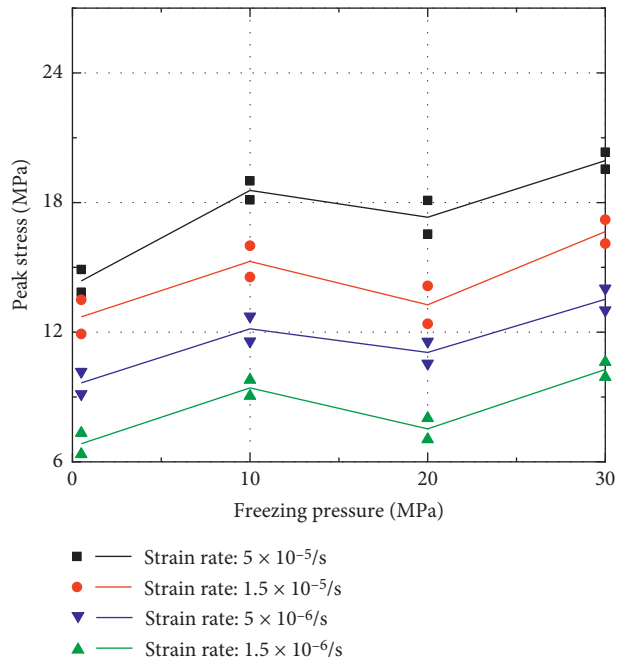

Figure 10: Variation in the peak stress with freezing pressure under different strain rates.

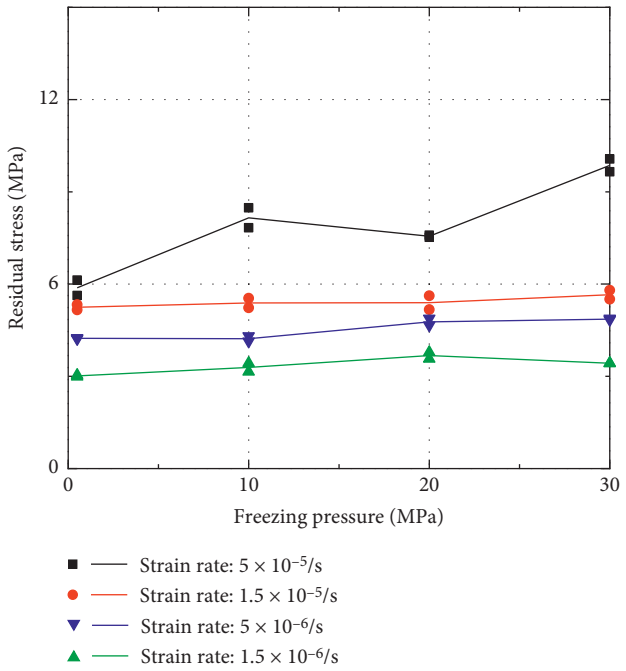

Figure 11: Variation in the residual stress with freezing pressure under different strain rates.

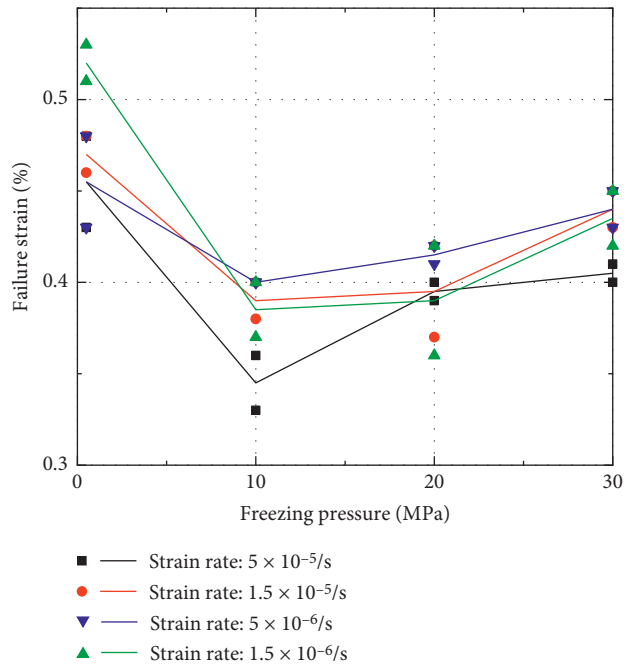

FIGURE 12: Variation in the failure strain with freezing pressure under different strain rates.

the failure strain of deep ice can be reduced by 26% as compared to that of shallow ice. The convergence deformation of the frozen wall should be strictly limited to prevent the rapid decline of its bearing capacity.

4. Conclusion

In this study, an effective method was proposed to prepare standard ice specimens under high hydraulic pressure in a triaxial pressure chamber. Using this technique, the in situ uniaxial compression test of ice specimens with temperature of 20°C and freezing pressure range of 0.5–30 MPa was carried out. The strain rate range was 5×10^{-5}-1.5×10^{-6} s^{-1}. The main results of the study are summarized as follows:

(1) The proposed specimen preparation technique continuously controls the stress state of the specimen during the entire process of freezing and testing, which was suitable for the in situ mechanical test of pressurized freezing ice. The geometric accuracy and temperature distribution of the prepared specimens met the test specifications.

(2) The failure modes of ice specimens changed from shear failure to splitting failure with the increase in the freezing pressure. The influence of freezing pressure on the failure characteristics of ice specimens was similar to that of low temperature, and the ductile-brittle transition zone moved to a slow strain rate range.

(3) The variation trends of brittleness index and peak stress of ice specimens with the freezing pressure were similar: both increased first, then decreased, and then again increased. However, the locations of extreme points are different. The values of brittleness index increased in the following order: (20 MPa) < (0.5 MPa) < (10 MPa) < (30 MPa), while the value relation of the peak stress is σ_p (0.5 MPa) < σ_p (20 MPa) < σ_p (10 MPa) < σ_p (30 MPa).

(4) When the ice specimen exhibited brittle failure, the influence of freezing pressure on residual stress is consistent with that of the peak stress. When the ice specimen exhibited ductile failure, there was no obvious relationship between the residual stress and freezing pressure.

(5) The failure strain of ice specimen first decreased and then increased with the increase in the freezing pressure, and the values increased in the following order: ε_p(10 MPa) < ε_p(20 MPa) < ε_p (30 MPa) < ε_p(0.5 MPa).

Data Availability

The data used to support the findings of the study are available from the corresponding author upon reasonable request.

Conflicts of Interest

The authors declare that they have no conflicts of interest.

Authors' Contributions

Baosheng Wang, Peixin Sun, and Yaodan Zhang performed the experiments; Baosheng Wang and Xin Huang analyzed the test data; Baosheng Wang and Fengjun Chen wrote the manuscript; Weihao Yang conceived the experiment and provided the guidance and suggestion.

Acknowledgments

This research was supported by the National Natural Science Foundation of China (Grant no. 51874286).

References

[1] T. Wang, H. Zhang, G. Q. Zhou, and X. Liu, "Evaluation of variability characteristics of mechanical parameters of artificially frozen clay in deep alluvium," *Cold Regions Science and Technology*, vol. 171, 2020.

[2] J. P. Wang, W. M. Liu, and H. Wang, "Comparisons on ground freezing constructions in 1000 m depth mine shafts," *Mine Construction Technology*, vol. 38, no. 4, pp. 34–37, 2017.

[3] B. Zhang, W. H. Yang, and B. S. Wang, "Elastoplastic design theory for ultra-deep frozen wall considering large deformation features," *Chinese Journal of Geotechnical Engineering*, vol. 41, no. 7, pp. 1288–1295, 2019.

[4] R. L. Shan, Y. Bai, L. Song et al., "Experimental study of blasting vibration and damage characteristics on frozen shaft wall," *Chinese Journal of Rock Mechanics and Engineering*, vol. 34, pp. 3732–3741, 2015, S3 in Chinese.

[5] R. Margesin, *Permafrost Soils*, Springer, New York, NY, USA, 2008.

[6] R. Atlasov, M. Nikolaeva, and V. Karamzin, *Drilling and Installation of Boreholes for Permafrost Thermal Monitoring on Livingston Island in the Maritime Antarctic*, 2019.

[7] D.-y. Wang, W. Ma, X.-x. Chang, and A. g. Wang, "Study on the resistance to deformation of artificially frozen soil in deep alluvium," *Cold Regions Science and Technology*, vol. 42, no. 3, pp. 194–200, 2005.

[8] Y. Yang, Y. Lai, and X. Chang, "Laboratory and theoretical investigations on the deformation and strength behaviors of artificial frozen soil," *Cold Regions Science and Technology*, vol. 64, pp. 39–45, 2010.

[9] D. Li, C. Zhang, G. Ding et al., "Fractional derivative-based creep constitutive model of deep artificial frozen soil," *Cold Regions Science and Technology*, vol. 170, 2020.

[10] Y. Bai, R. Shan, Y. Jua, Y. Wu, P. Sun, and Z. Wang, "Study on the mechanical properties and damage constitutive model of frozen weakly cemented red sandstone," *Cold Regions Science and Technology*, vol. 171, 2020.

[11] L. Wang, N. Li, J. Qi, Y. Tian, and S. Xu, "A study on the physical index change and triaxial compression test of intact hard rock subjected to freeze-thaw cycles," *Cold Regions Science and Technology*, vol. 160, pp. 39–47, 2019.

[12] C. Zhu, M. C. He, X. H. Zhang, Z. G. Tao, Q. Lin, and L. f. Li, "Nonlinear mechanical model of constant resistance and large deformation bolt and influence parameters analysis of constant resistance behavior," *Rock and Soil Mechanics*, vol. 42, no. 7, pp. 1911–1924, 2021, in Chinese.

[13] Q. Yin, J. Y. Wu, C. Zhu, M. He, Q. Meng, and H. Jing, "Shear mechanical responses of sandstone exposed to high temperature under constant normal stiffness boundary conditions," *Geomechanics and Geophysics for Geo-Energy and Geo-Resources*, vol. 7, no. 35, 2021.

[14] F. Wu, H. Zhang, Q. L. Zou, C. Li, J. Chen, and R. Gao, "Viscoelastic-plastic damage creep model for salt rock based on fractional derivative theory," *Mechanics of Materials*, vol. 150, 2020.

[15] M. J. Siegert, K. Kwok, and C. Mayer, "Water exchange between subglacial Lake Vostok and the overlying ice sheet," *Nature*, vol. 403, pp. 643–646, 2000.

[16] V. Lukin and S. Bulat, "Vostok subglacial lake: details of Russian plans/activities for drilling and sampling," *Geophysical Monograph Series*, vol. 192, pp. 187–197, 2011.

[17] J. Jouzel, J. R. Petit, R. Souchez et al., "More than 200 meters of lake ice above subglacial lake vostok, Antarctica," *Science*, vol. 286, no. 5447, pp. 2138–2141, 1999.

[18] M. H. Carr, M. J. S. Belton, C. R. Chapman et al., "Evidence for a subsurface ocean on Europa," *Nature*, vol. 391, pp. 363–365, 1998.

[19] S. J. Jones, "A review of the strength of iceberg and other freshwater ice and the effect of temperature," *Cold Regions Science and Technology*, vol. 47, pp. 256–262, 2007.

[20] L. W. Gold, "Some observations on the dependence of strain on stress for ice," *Canadian Journal of Physics*, vol. 36, no. 10, pp. 1265–1275, 1958.

[21] L. W. Gold, "The elastic modulus of columnar-grain freshwater ice," *Annals of Glaciology*, vol. 19, pp. 13–18, 1994.

[22] A. Traelleberg, L. W. Gold, and R. Frederking, *The Strain Rate and Temperature Dependence of Young's Modulus of Ice*, U.S. Army Cold Regions Research and Engineering Laboratory, Hanover, NH, USA, 1975.

[23] N. K. Sinha, "Rate sensitivity of compressive strength of columnar-grained ice," *Experimental Mechanics*, vol. 21, no. 6, pp. 209–218, 1981.

[24] G. A. Kuehn and M. S. E. ", "The mechanical properties of saline ice under uniaxial compression," *Annals of Glaciology*, vol. 19, pp. 39–48, 1994.

[25] J. R. Rice and R. Thomson, "Ductile versus brittle behaviour of crystals," *Philosophical Magazine*, vol. 29, no. 1, pp. 73–97, 1974.

[26] E. M. Schulson and S. E. Buck, "The ductile-to-brittle transition and ductile failure envelopes of orthotropic ice under biaxial compression," *Acta Metallurgica et Materialia*, vol. 43, no. 10, pp. 3661–3668, 1995.

[27] G. Timco and R. Frederking, "Comparative strengths of fresh water ice," *Cold Regions Science and Technology*, vol. 6, no. 1, pp. 21–27, 1982.

[28] M. Arakawa and N. Maeno, "Mechanical strength of polycrystalline ice under uniaxial compression," *Cold Regions Science and Technology*, vol. 26, no. 3, pp. 215–229, 1997.

[29] W. F. Weeks and G. F. N. Cox, *Laboratory Preparation of Artificial Sea and Salt Ice*, Cold Regions Research and Engineering Laboratory, Hanover, NH, U.S.A, 1974.

[30] T. R. Smith and E. M. Schulson, "The brittle compressive failure of fresh-water columnar ice under biaxial loading," *Acta Metallurgica et Materialia*, vol. 41, no. 1, pp. 153–163, 1993.

[31] G. A. Kuehn, R. W. Lee, W. A. Nixon, and E. M. Schulsan, "The structure and tensile behavior of first-year sea ice and laboratorygrown saline ice," *Journal of Offshore Mechanics and Arctic Engineering*, vol. 112, no. 4, pp. 357–363, 1990.

[32] I. L. Meglis, R. E. Gagnon, and R. P. Young, "Microcracking during stress-relief of polycrystalline ice formed at high pressure," *Geophysical Research Letters*, vol. 22, no. 16, pp. 2207–2210, 1995.

[33] B. S. Wang, P. X. Sun, T. T. Luo et al., *Freezing Pressurized Water into a Standard Cylindrical Ice Sample in a Triaxial Cell*, Geofluids, 2021.

[34] V. Petrenko and R. Whitworth, *Physics of Ice*, Oxford University Press, Oxford, England, 2002.

[35] R. Ulusay, *The ISRM Suggested Methods for Rock Characterization, Testing and Monitoring: 2007-2014*, Springer International Publishing, New York, NY, USA, 2015.

[36] S. Snyder and J. S. Franks, "Quantifying the effects of sensor coatings on body temperature measurements," *Animal Biotelemetry*, vol. 4, 2016.

[37] Q. Wang, M. C. He, S. C. Li et al., "Comparative study of model tests on automatically formed roadway and gob-side entry driving in deep coal mines," *International Journal of Mining Science and Technology*, vol. 31, no. 4, pp. 591–601, 2021.

[38] Q. Wang, Y. Wang, M. C. He et al., "Experimental research and application of automatically formed roadway without advance tunneling," *Tunnelling and Underground Space Technology*, vol. 114, 2021.

[39] P. Kalifa, G. Ouillon, and P. Duval, "Microcracking and the failure of polycrystalline ice under triaxial compression," *Journal of Glaciology*, vol. 38, no. 128, pp. 65–76, 1992.

[40] M. L. Couture and E. M. Schulson, "The cracking of ice during rapid unloading," *Philosophical Magazine Letters*, vol. 69, no. 1, pp. 9–14, 1994.

[41] S. J. Jones, "Comparison of the strength of iceberg and other freshwater ice and the effect of temperature," National Research Council of Canada. NRC Institute for Ocean Technology, Newfoundland, Canada, 2006.

[42] S. J. Jones, "The confined compressive strength of polycrystalline ice," *Journal of Glaciology*, vol. 28, no. 98, pp. 171–178, 1982.

[43] D. M. Cole, "Strain-rate and grain-size effects in ice," *Journal of Glaciology*, vol. 115, no. 33, pp. 274–280, 1987.

[44] I. Meglis, *High Speed Testing of Freshwater Granular Ice*, Institute for Marine Dynamics, National Research Council of Canada, Ottawa, Canada, 1998.
[45] R. O. Ramseier, *Growth and Mechanical Properties of River and lake Ice*, Laval University, Quebec, Canada, 1976.
[46] G. Feng, Y. Kang, X. C. Wang, Y. Wu, and X. Li, "Investigation on the failure characteristics and fracture classification of shale under Brazilian test conditions," *Rock Mechanics and Rock Engineering*, vol. 53, no. 7, pp. 3325–3340, 2020.
[47] G. Feng, X. C. Wang, M. Wang, and Y. Kang, "Experimental investigation of thermal cycling on fracture characteristics of granite in a geothermal-energy reservoir," *Engineering Fracture Mechanics*, vol. 235, 2020.
[48] A. W. Bishop, *Progressive Failure with Special Reference to the Mechanism Causing it*, Oslo, Oslo, Norway, 1967.
[49] H. Zhou, F. Z. Meng, C. Q. Zhang, R. Xu, and J. Lu, "Quantitative evaluation of rock brittleness based on stress-strain curve," *Chinese Journal of Rock Mechanics and Engineering*, vol. 33, no. 6, pp. 1114–1122, 2014, in Chinese.
[50] Y. J. Xia, L. C. Li, C. A. Tang et al., "Rock brittleness evaluation based on stress dropping rate after peak stress and energy ratio," *Chinese Journal of Rock Mechanics and Engineering*, vol. 35, no. 6, pp. 1141–1154, 2016, in Chinese.
[51] B. Tarasov and Y. Potvin, "Universal criteria for rock brittleness estimation under triaxial compression," *International Journal of Rock Mechanics and Mining Sciences*, vol. 59, pp. 57–69, 2013.
[52] M. Mellor and D. M. Cole, "Deformation and failure of ice under constant stress or constant strain-rate," *Cold Regions Science and Technology*, vol. 5, no. 3, pp. 201–219, 1982.
[53] Z. C. Duan, "Deep and ultra-deep karst," *Geological Science and Technology Information*, vol. S1, pp. 122–124, 1982, in Chinese.
[54] Y. K. Yang, J. J. Zheng, and Q. H. Fang, "Application of freezing method in pile foundation of bridge," *Bridge Construction*, vol. 2, pp. 54–56, 2002, in Chinese.
[55] R. Frederking, "Plane-strain compressive strength of columnar-grained and granular-snow ice," *Journal of Glaciology*, vol. 18, no. 80, pp. 505–516, 1977.